Technical Point of View

Cardiac and Respiratory Motion-induced Artifact in Myocardial Perfusion SPECT: 4D Digital Anthropomorphic Phantom Study

Koichi Okuda, PhD[1], Kenichi Nakajima, MD[2], Akihiro Kikuchi, PhD[3], Masahisa Onoguchi, PhD[4] and Mitsumasa Hashimoto, PhD[1]

Received: February 1, 2017/Revised manuscript received: May 8, 2017/Accepted: May 16, 2017
J-STAGE Advance published: July 14, 2017

Abstract

***Background*: Digital anthropomorphic phantoms have gradually gained an important role in nuclear medicine imaging. The aim of this study was to generate digital phantom models simulated with cardiac and respiratory motions and to evaluate motion-induced artifact using a quantitative software program developed with artificial intelligence (AI) technology in myocardial perfusion single-photon emission computed tomography (SPECT) images.**

***Methods*: A digital anthropomorphic torso phantom and Monte Carlo simulation program were used to generate the projection image. We prepared electrocardiographic- and respiratory-gated models with cardiac and respiratory motions in the diaphragmatic motion of 0-50 mm and chest anterior-posterior (AP) expansion of 0-30 mm. The phantoms had ^{99m}Tc radiopharmaceuticals embedded based on a normal male subject. The projection data were reconstructed with filtered back projection method. The 17-segment polar map without attenuation correction was created. Myocardial count ratio was calculated in the anterior and inferior walls to the anterolateral wall on the polar map.**

***Results*: The low myocardial perfusion distribution was clearly observed in the basal to mid anterior and inferior walls, when the diaphragmatic motion and AP expansion were increased. The anterior and inferior count ratios showed significant decrease with diaphragmatic motion (≥30 mm) compared to without diaphragmatic motion (0.71 ± 0.05 vs. 0.76 ± 0.06; $p<0.0001$, 0.67 ± 0.04 vs. 0.69 ± 0.04; $p=0.038$, respectively). The anterior and inferior motion artifacts could not be detected by the quantitative software program in the diaphragm motion of ≤20 mm and AP expansion of ≤12 mm.**

***Conclusions*: The cardiac and respiratory motion-induced artifacts were characterized as low anterior and inferior myocardial counts. Therefore, motion artifacts should be considered when we observe this sort of count decreases on the reconstructed images and polar maps. However, we could exclude the mild motion-induced artifacts by using the quantitative software program integrated with AI technology.**

Keywords: Cardiac motion, Digital phantom, Monte Carlo simulation, Myocardial perfusion SPECT, Respiratory motion

Ann Nucl Cardiol 2017；3（1）：88-93

The acrylic anthropomorphic phantoms can hardly simulate electrocardiographic- and respiratory-gated patient studies in myocardial perfusion single-photon emission computed tomography (SPECT) influenced by cardiac and respiratory movements. In this decade, the digital phantom has gradually gained an important role in medical imaging (1-5),

doi: 10.17996/anc.17-00005

1) Koichi Okuda, Mitsumasa Hashimoto
Department of Physics, Kanazawa Medical University, 1-1 Daigaku, Uchinada, Kahoku, Ishikawa 920-0293, Japan
E-mail: okuda@kanazawa-med.ac.jp
2) Kenichi Nakajima
Department of Nuclear Medicine, Kanazawa University Hospital, Kanazawa, Japan
3) Akihiro Kikuchi
Department of Radiological Technology, Hokkaido University of Science, Sapporo, Japan
4) Masahisa Onoguchi
Department of Quantum Medical Technology, Kanazawa University, Kanazawa, Japan

Table 1 Parameters for digital phantom and Monte Carlo simulation program

Digital phantom		Simulation program	
Structure		Radiopharmaceutical	
Phantom size [voxel]	256×256×256	Photon energy [keV]	140
Voxel size [mm]	2.0	Activity [MBq]	370
RI Activity [activity/voxel]		Camera and collimator	
Left and right ventricle	100	Crystal Size [mm]	223×296
Liver	20	Crystal Thickness [cm]	0.95
Lung	10	Energy resolution [%]	10
Cardiac motion		Intrinsic resolution [cm]	0.34
Cardiac cycle [sec]	1	Collimator	LEHR
Bin per cycle	8	SPECT acquisition	
Respiratory motion		Energy window [keV]	140±7.5%
Respiratoy cycle [sec]	5	Camera rotation [deg]	360
Bin per cycle	5	Imaging matrix	64×64
AP expansion [mm]	12	Pixel size [mm]	6.6
Diaphragm motion [mm]	20	Projection bin	60

Abbreviations: AP: anterior-posterior, LEHR: low-energy high resolution

and it can mathematically simulate anatomical organ movement in nuclear medicine imaging. Moreover, high-resolution cardiac and respiratory motions can be simulated using clinical gated computed tomography (CT) data in state-of-the-art digital anthropomorphic phantom (1).

Respiratory motion has been measured and its correction has been performed to compensate motion artifacts in clinical myocardial perfusion SPECT (MPS) imaging (6,7). Moreover, digital phantom study has also been performed to demonstrate motion-induced artifacts, and this study characterized the extent and severity of motion-induced artifacts (8). The digital phantom study is especially important for assessment of relationship between the amplitude of respiratory motion and motion-induced artifacts as well as the development and evaluation of a motion-correction method.

The aim of this study was to demonstrate motion-induced artifacts using a digital anthropomorphic phantom and to clarify the relationship between cardiac and respiratory motion-induced artifacts in MPS images and the amplitude of diaphragmatic motion and chest expansion. Moreover, we evaluated MPS images influenced by cardiac and respiratory motions by using a dedicated software program integrated with artificial intelligence (AI) technology.

Methods

We created four digital anthropomorphic torso models using four-dimensional (4D) extended cardiac-torso (XCAT) phantom (Duke University, Durham, USA) (1). These models simulated a male patient whose height is 171 cm. A static model and gated models with either cardiac motion or respiratory motion, and that with both cardiac and respiratory motions were created. These digital phantoms simulated ^{99m}Tc radiopharmaceutical activity distribution of the heart, liver and lung for a normal subject. The left ventricular (LV) end-diastolic volume and ejection fraction were set as 132 mL and 61%, respectively. Numerical parameters for generating digital phantoms are shown in Table 1. Additionally six gated models were created using the XCAT phantom. These models simulated cardiac and respiratory motions (0-50 mm diaphragmatic and 0-30 mm anterior-posterior (AP) chest expansion)

Using the Simulation of Imaging Nuclear Detectors (SIMIND) Monte Carlo program (9), projection datasets were generated from the digital phantom models. Numerical parameters for projection data creation are shown in Table 1. The projection data were reconstructed with filtered back projection method. Attenuation correction was not used in this study. Polar maps were created with the Heart Score View software program (Nihon Medi-Physics Co., Ltd., Tokyo, Japan). Myocardial count ratios of the anterior and inferior walls to the anterolateral wall were calculated. The anterior, inferior, and anterolateral myocardial counts were calculated as mean values in the segments 1 and 7, segments 4 and 10, and segments 12 and 16 on American Heart Association classification of the polar map (10), respectively. We used cardioREPO (cREPO; FUJIFILM RI Pharma, Tokyo, Japan) software program integrated with an artificial neural network (ANN) feature for evaluation of myocardial perfusion and compensation of small-heart effect (11-14). This software program automatically creates diagnosis based on the probability of perfusion abnormality using ANN trained by expert nuclear medicine physicians and cardiologists. The

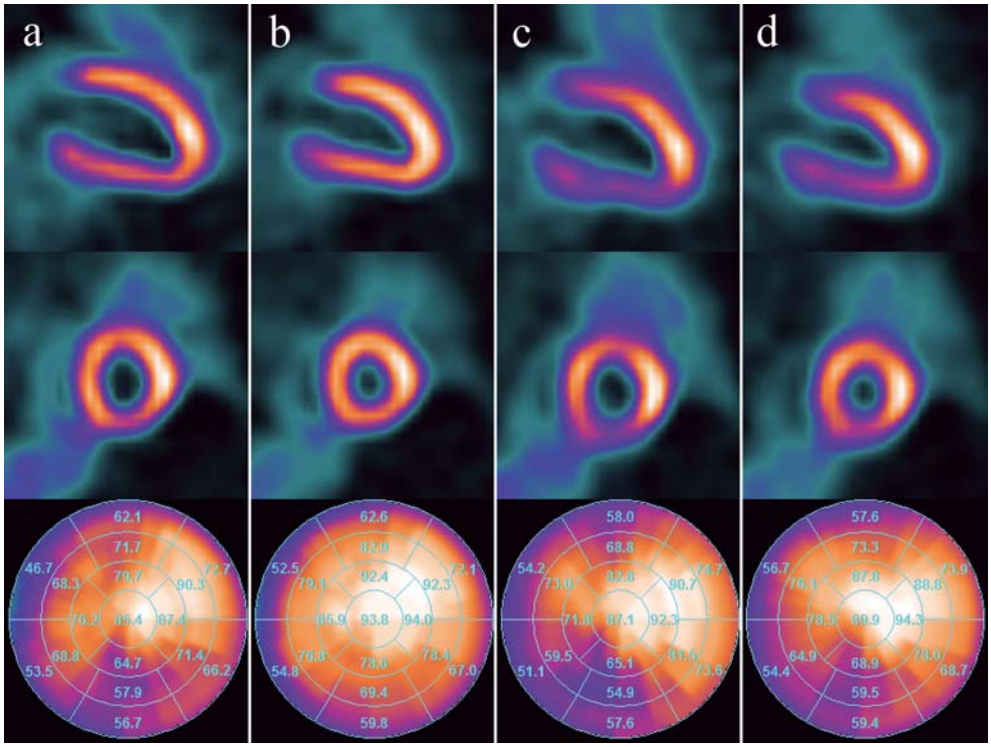

Fig. 1 Vertical long-axis (top) and short-axis (middle) views of MPS images derived from four phantom models: static model (**a**), gated model with cardiac motion (**b**), gated model with respiratory motion (**c**), and gated model with both cardiac and respiratory motions (**d**). Polar maps segmented into 17 regions were created from the four phantom models (bottom).

probability of perfusion abnormality was given as ANN values ranged from 0 to 1.0, corresponding to definitely normal perfusion to abnormal perfusion.

All continuous values were expressed as the mean ± standard deviation. A student's t-test and paired t-test were used to analyze the differences in continuous variables. To analyze the multiple comparisons, the analysis of variance test and Tukey-Kramer comparison method were used. All statistical tests were two-tailed, and a p value < 0.05 was considered significant. These analyses were performed by using JMP version 11.2.1 (SAS Institute Inc., Cary, NC, USA).

Results

The vertical long-axis (VLA) and short-axis (SA) views of MPS images were generated from four phantom models (Fig. 1). In the MPS images derived from the static phantom, the diaphragm and liver attenuated ^{99m}Tc myocardial counts in the inferior wall (Fig. 1a). Although the gated model with cardiac motion provided uniform myocardial count distribution, a decreased LV chamber volume was clearly observed (Fig. 1b). The craniocaudal movement of the heart by respiratory motion caused low myocardial counts in the anterior and inferior walls (Fig. 1c). The low anterior and inferior myocardial count distributions were characterized in the polar map, and small LV chamber volume was observed in the gated phantom model included with cardiac and respiratory motions, (Fig. 1d). Myocardial count distributions were different in the polar maps generated from four phantom models. However, the myocardial count distribution was consistently high in the apical lateral and mid anterolateral segments (87.4－94.3%).

The myocardial count ratios of the anterior and inferior walls to the anterolateral wall were calculated on the polar map (Fig. 2a). The anterior count ratio was significantly increased in the gated model with cardiac motion in comparison to the static model (0.77 ± 0.07 vs. 0.73 ± 0.08, $p<0.01$). The anterior count ratio was significantly decreased in the gated model with respiratory motion in comparison to the static model (0.69 ± 0.06 vs. 0.73 ± 0.08, $p<0.001$). However, there was no difference in the anterior count ratios derived from the static model and the gated model with cardiac and respiratory motions. Regarding the inferior count ratio, the gated model with cardiac motion and that with cardiac and respiratory motions exhibited significantly higher values in comparison to the static model (0.68 ± 0.04 and 0.66 ± 0.09 vs. 0.63 ± 0.06, $p<0.0001$ and $p<0.05$, respectively). However, there was no difference in the inferior count ratios derived from the static model and the gated model with respiratory motion.

The relationship between myocardial count ratios in the anterior and inferior walls on the polar map and the amplitude of respiratory motions was shown in Fig. 2b. When the

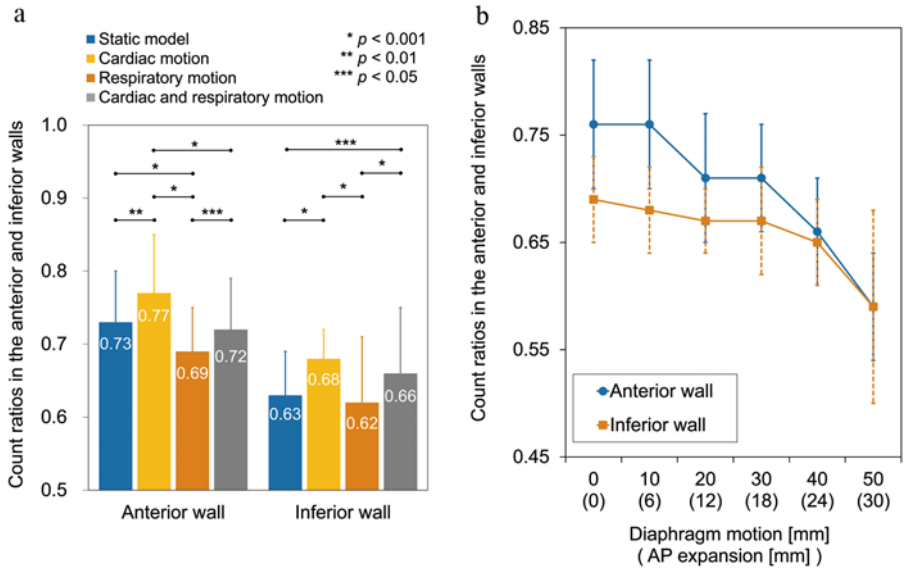

Fig. 2 **a**: Myocardial count ratios of the anterior and inferior walls to the anterolateral wall. Myocardial count ratios were calculated in four digital phantom models: static model (blue bars), gated model with cardiac motion (yellow bars), gated model with respiratory motion (orange bars), and gated model with both cardiac and respiratory motions (gray bars). **b**: The relationship between myocardial count ratio in the anterior and inferior walls on the polar map and the amplitude of respiratory motions simulated with 6 digital phantom models. The diaphragmatic motion changed from 0 mm to 50 mm, and AP expansion changed from 0 mm to 30 mm. The blue line and orange line showed count ratio changes in the anterior and inferior walls, respectively.

diaphragmatic motion and AP expansion were increased, the anterior and inferior count ratios were gradually decreased. The anterior count ratio showed significant decrease in the diaphragmatic motion of 20, 30, 40, and 50 mm in comparison to that without diaphragmatic motion ($p<0.0001$). Regarding the inferior count ratio, significantly decreased value was also exhibited in the diaphragmatic motion of 30, 40, and 50 mm in comparison to that without diaphragmatic motion ($p<0.05$).

A total of 6 polar map views of myocardial count distributions were generated from 6 digital phantom models simulated with cardiac and respiratory motions (Fig. 3). The cREPO software program automatically detected the area of myocardial count abnormality in the anterior and inferior walls (Fig. 3d, e, f). When the diaphragmatic motion and AP expansion were set as 30 mm and 18 mm, respectively, respiratory motion-induced artifact appeared in the Inferior wall. Moreover, respiratory motion-induced artifact in the anterior wall also appeared in the diaphragmatic motion of 40 mm and AP expansion of 24 mm. The severity of motion artifacts was determined as mild abnormal perfusion in the all areas by using the cREPO software program. The ANN values showed 0.76 for the inferior wall in Fig. 3d, 0.59 and 0.86 for the anterior and inferior walls, respectively, in Fig. 3e, and 0.71 and 0.97 for the anterior and inferior walls, respectively, in Fig. 3f.

Discussion

Using the digital phantom and Monte Carlo simulation program, MPS images were created, and cardiac and respiratory motion-induced artifacts were evaluated. When the diaphragmatic motion and chest expansion were increased, the anterior and inferior count ratios were gradually decreased. Although the motion-induced artifacts were observed in the anterior and inferior walls of the phantom models with the 20 mm-diaphragmatic motion and 12 mm-AP expansion, the cREPO software program determined anterior and inferior low myocardial counts as normal distributions.

Segars et al. also reported that a low myocardial perfusion influenced by both cardiac and respiratory motions was seen in the anterior and inferior walls in a digital phantom study (2). Moreover, Polycarpou et al. performed a gated real phantom scan to assess the motion-induced artifacts (15). A low myocardial count distribution influenced by respiratory motion was observed in the anterior and inferior walls in both studies. These results demonstrated that increased partial volume loss in the anterior and inferior walls that were orthogonal to the direction of respiratory motion, and consequently motion-induced defects in the both walls were appeared. Moreover, the respiratory motion correction could compensate for artifacts and provide uniform myocardial count distribution.

The extent and severity of myocardial perfusion defects due

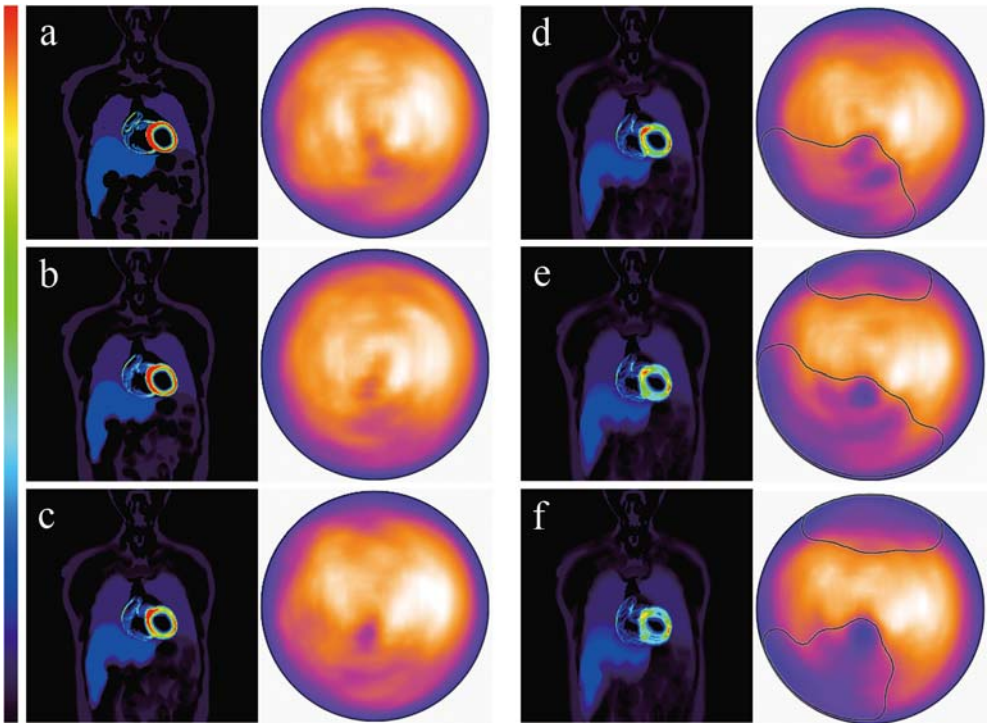

Fig. 3 Coronal views of 6 digital anthropomorphic torso phantoms and polar map views of myocardial count distributions. Diaphragmatic motion and AP expansion were set as 0 mm (**a**), 10 mm and 6 mm (**b**), 20 mm and 12 mm (**c**), 30 mm and 18 mm (**d**), 40 mm and 24 mm (**e**), and 50 mm and 30 mm (**f**), respectively. The cREPO software program integrated with the AI technology automatically detected abnormal perfusion areas surrounded by black line in panels (d), (e), and (f).

to respiratory motion varied depending on the amplitude of diaphragmatic motion and AP expansion. We can't distinguish respiratory motion-induced artifacts and attenuated radiopharmaceutical concentration in the inferior wall. However, if particular defects in the both anterior and inferior walls are simultaneously observed, motion-induced artifacts should be taken into consideration during clinical interpretation. Lee et al. also performed digital phantom study to evaluate the respiratory motion-induced artifacts, and the anterior artifacts disappeared in the end-inhalation and end-exhalation phases (8). SPECT acquisitions at end-inhalation and end-exhalation phases can be helpful to rule out respiratory motion induced artifacts when we can perform high–speed cardiac MPS imaging by using the cadmium zinc telluride gamma camera.

Conclusions

We performed digital anthropomorphic torso phantom study to simulate cardiac and respiratory motion in SPECT acquisition. The cardiac and respiratory motion-induced artifacts were simulated in MPS images and characterized as low anterior and inferior myocardial counts. Therefore, motion artifacts should be considered when this type of pattern is observed. However, the cREPO software program determined these motion-induced artifacts as a normal myocardial perfusion distribution in the digital phantom models with the diaphragmatic motion of ≤20 mm and AP expansion of ≤12 mm.

Acknowledgment

The authors thank Takayuki Shibutani MSc, Hiroto Yoneyama Ph.D, Shinro Matsuo MD of Kanazawa University, Kanazawa, Japan for assistances from the viewpoint of technical and clinical aspects. The authors also thank Segars WP Ph.D of Duke University Medical Center, Durham, NC, USA for 4D XCAT digital phantom study.

Sources of funding

This study was partly funded by the JSPS KAKENHI Grants (Numbers 26861022) and the Grants for Promoted Research from the Kanazawa Medical University (S2014-13 and S2016-6).

Conflicts of interest

None.

Reprint requests and correspondence:
Koichi Okuda, PhD
Department of Physics, Kanazawa Medical University 1-1 Daigaku, Uchinada, Kahoku, Ishikawa 920-0293, Japan
E-mail: okuda@kanazawa-med.ac.jp

References

1. Segars WP, Sturgeon G, Mendonca S, et al. 4D XCAT phantom for multimodality imaging research. Med Phys 2010; 37: 4902-15.
2. Segars WP, Tsui BM. Study of the efficacy of respiratory gating in myocardial SPECT using the new 4D NCAT phantom. IEEE Trans Nucl Sci 2002; 49: 675-9.
3. Murakami T, Hashimoto J, Hara T, et al. Development of digital myocardial phantom to evaluate software for gated SPECT. Ann Nucl Cardiol 2015; 1: 61-8.
4. Maeda H, Yamaki N, Azuma M. Development of the software package of the nuclear medicine data processor for education and research. Nihon Hoshasen Gijutsu Gakkai Zasshi 2012; 68: 299-306.
5. Zubal IG, Harrell CR, Smith EO, et al. Computerized three-dimensional segmented human anatomy. Med Phys 1994; 21: 299-302.
6. Kovalski G, Israel O, Keidar Z, et al. Correction of heart motion due to respiration in clinical myocardial perfusion SPECT scans using respiratory gating. J Nucl Med 2007; 48: 630-6.
7. Cho K, Kumiata S, Okada S, et al. Development of respiratory gated myocardial SPECT system. J Nucl Cardiol 1999; 6: 20-8.
8. Lee TS, Tsui BM. The development and initial evaluation of a realistic simulated SPECT dataset with simultaneous respiratory and cardiac motion for gated myocardial perfusion SPECT. Phys Med Biol 2015; 60: 1399-413.
9. Ljungberg M, Strand S-E, King MA. Monte Carlo calculations in nuclear medicine, second edition: Applications in diagnostic imaging: CRC Press, 2012.
10. Cerqueira MD, Weissman NJ, Dilsizian V, et al. Standardized myocardial segmentation and nomenclature for tomographic imaging of the heart. A statement for healthcare professionals from the Cardiac Imaging Committee of the Council on Clinical Cardiology of the American Heart Association. Circulation 2002; 105: 539-42.
11. Nakajima K, Matsuo S, Wakabayashi H, et al. Diagnostic performance of artificial neural network for detecting ischemia in myocardial perfusion imaging. Circ J 2015; 79: 1549-56.
12. Nakajima K, Okuda K, Nystrom K, et al. Improved quantification of small hearts for gated myocardial perfusion imaging. Eur J Nucl Med Mol Imaging 2013; 40: 1163-70.
13. Johansson L, Edenbrandt L, Nakajima K, et al. Computer-aided diagnosis system outperforms scoring analysis in myocardial perfusion imaging. J Nucl Cardiol 2014; 21: 416-23.
14. Edenbrandt L, Höglund P, Frantz S, et al. Area of ischemia assessed by physicians and software packages from myocardial perfusion scintigrams. BMC Med Imaging 2014; 14: 5.
15. Polycarpou I, Chrysanthou-Baustert I, Demetriadou O, et al. Impact of respiratory motion correction on SPECT myocardial perfusion imaging using a mechanically moving phantom assembly with variable cardiac defects. J Nucl Cardiol 2015. [Epub ahead of print]